BioChip J. (2018) 12(1): 11-17
DOI 10.1007/s13206-017-2102-2

Original Article

Label-free Microarray-based Binding Affinity Constant Measurement with Modified Fluidic Arrangement

Junwei Hu[1], Ru Chen[2], Chenggang Zhu[2], Bilin Ge[2], Xiangdong Zhu[3], Lan Mi[2], Jiong Ma[2], Caiqin Han[1], Hao Chen[1,*] & Yiyan Fei[2,*]

Received: 06 July, 2017 / Accepted: 15 August, 2017 / Published online: 13 March, 2018

Abstract The oblique-incidence reflectivity difference (OI-RD) scanning microscopy has the capability of simultaneously measuring binding curves of a protein probe with tens of thousands molecular targets in a microarray and yielding reaction rate constants. However, the quality of reaction rate constants is influenced by the fluidic system. To improve the quality of reaction rate constant measurement over the entire microarray, we demonstrate a fluidic chamber that allows the fluid to flow from the bottom to the top uniformly across the microarray and thus provides more uniform and accurate measurements of reaction rate constants with simplified fluidic design.

Keywords: Optical biosensors, Protein microarray, Kinetics measurement, Affinity constant

Introduction

Microarrays consist of 10^2-10^6 immobilized targets as distinct features on a solid support and allow the targets simultaneously exposed to a probe solution of interest so that binding reactions of the probe with all targets are assayed at the same time[1]. Microarrays have emerged as a leading high-throughput technology for system biology research such as genomics[1,2] proteomics[3,4], glycomics[5,6], transcriptomics[7,8], metabolomics[9,10]. The fluorescence-based detection of microarray is widely used for its superior sensitivity[11]. However, fluorescence labeling a protein probe inevitably changes innate properties of the protein[12]. In addition fluorescence-based methods provide only endpoint information on binding reactions instead of kinetics rate constants and information on the thermodynamics. Optical biosensors, such as surface plasmon resonance (SPR)[13,14], reflection interference spectroscopy[15,16], dielectric wave guide reflectometry[17], and imaging ellipsometry[18,19], have been developed to complement the fluorescence-based detection by providing both endpoint image and kinetic measurements of binding reactions without extrinsic labels[20,21]. Oblique-incidence reflectivity difference (OI-RD) scanning microscopy is an ellipsometry-based optical biosensor which is capable of simultaneous measurement of binding curves of a probe with tens of thousands of targets immobilized on a functionalized glass surface[22,23]. When a solution or a buffer is introduced to the chamber to flow across the microarray, the fluid exchange around corners of the chamber is often insufficient and in turn causes inaccurate measurements of binding kinetics constants in these locations[22,23].

In this work, we present the development of a fluidic system which enables the liquid to flow from the bottom to the top of the fluidic chamber against gravity. With such fluidic design, OI-RD has a number of ad-

[1]Jiangsu Key Laboratory of Advanced Laser Materials and Devices, School of Physics and Electronic Engineering, Jiangsu Normal University, Xuzhou, 221116, China
[2]Department of Optical Science and Engineering, Shanghai Engineering Research Center of Ultra-Precision Optical Manufacturing, Key Laboratory of Micro and Nano Photonic Structures (Ministry of Education), Fudan University, Shanghai, 200433, China
[3]Department of Physics, University of California, Davis, California, 95616, USA
*Correspondence and requests for materials should be addressed to Y. Fei (✉fyy@fudan.edu.cn) and H. Chen (✉6019980049@jsnu.edu.cn)

vantages: (1) uniform equilibrium dissociation constants are achieved across the large microarray; (2) the fluidic system is cost effective by employing only one syringe pump and one liquid selection valve; (3) the time resolution of real-time binding curves can be improved by spending less time moving the mechanical stage.

Oblique-incidence Reflectivity Difference Scanning Microscope

As a special form of ellipsometry capable of measuring changes in an ultrathin film on the solid surface[24], the OI-RD technique has been successfully applied to studies of a wide variety of materials and surface processes, including ion sputtering and thermal annealing[25], gas adsorption[26], epitaxial growth[27], electrochemical deposition[28,29], and biosensing[24,30-36]. An arrangement of the scanning OI-RD microscope is shown in Figure 1. The laser is used as a monochromatic light source whose polarization state is modified and analyzed. A photo-elastic modulator (PEM) alters the polarization of the incident light beam at an angular frequency of $\Omega = 2\pi f_{PEM}$ ($f_{PEM} = 50$ kHz). The phase shifter introduces a static phase difference between *p*-polarized and *s*-polarized components of the light beam for nulling ellipsometry. The laser beam is focused with an f-theta lens on the back surface of the glass slide containing a microarray of interest at incident angle $\theta = 36.6°$. After reflection from the surface, the light beam passes the analyzer that mixes the two polarized components for polarization state analysis. The beam after the analyzer is detected with a photodiode and the output of the photodiode is analyzed with two lock-in amplifiers that yield the first and second harmonics of modulation frequency in the detected signal. When the film thickness d is much less than the wavelength λ, the ratio of the first harmonic amplitude to the second harmonic amplitude is essentially equal to the differential phase change between the *p*- and *s*-polarized components Δδ due to the change on the surface such as film thickness d,

$$\Delta\delta \cong \frac{-4\pi\sqrt{\varepsilon_s}\cos\theta}{(\varepsilon_0-\varepsilon_s)(\cot^2\theta-\varepsilon_s/\varepsilon_0)}\,\frac{(\varepsilon_d-\varepsilon_0)(\varepsilon_d-\varepsilon_s)}{\varepsilon_d}\,\frac{d}{\lambda} \quad (1)$$

ε_s, ε_0, and ε_d are the optical dielectric constants of the ambient, the solid substrate, and the molecular layer, respectively. By following Δδ in real time with the OI-RD technique, kinetics of surface processes such as film growth or biomolecular binding reactions can be measured[24].

For detection of binding reactions of a molecular probe with a microarray of immobilized targets under an aqueous condition, we built a flow cell as shown in Figure 2. A PEEK cap with a 0.5 mm deep fluidic chamber has an inlet at the bottom and an outlet on the top. A glass slide bearing large microarray is placed on the PEEK cap with an o-ring. A clamp fastens the PEEK cap and glass slide together to seal the fluidic chamber. In addition to the flow cell, the fluidic system consists of a syringe pump and a ten-way selection valve as shown in Figure 3. The inlet of the fluidic chamber connects to the central port of ten-way selection valve. The outlet of fluidic chamber connects to the syringe pump. When a liquid is pushed from the bottom to the top of a fluidic chamber, the liquid experiences the following forces: the upward force caused by the pressure difference, the gravity, the frictional force within the liquid and between the liquid and the

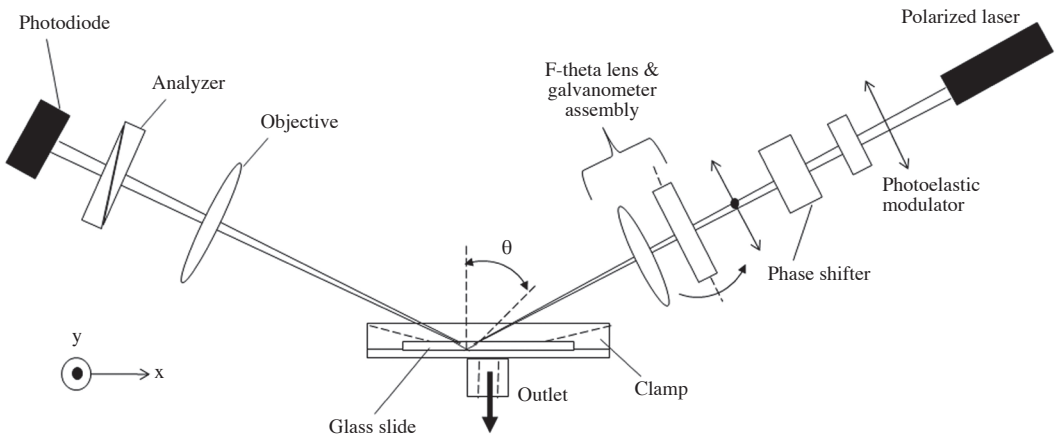

Figure 1. Optical layout of the scanning OI-RD microscope. Imaging of microarray is achieved by two-dimensional scanning which is composed of raster scanning of the focus beam across the microarray with a galvanometer along the y-axis (vertical direction) and moving of microarray fluidic assembly along the x-axis (horizontal direction) with a translation stage.

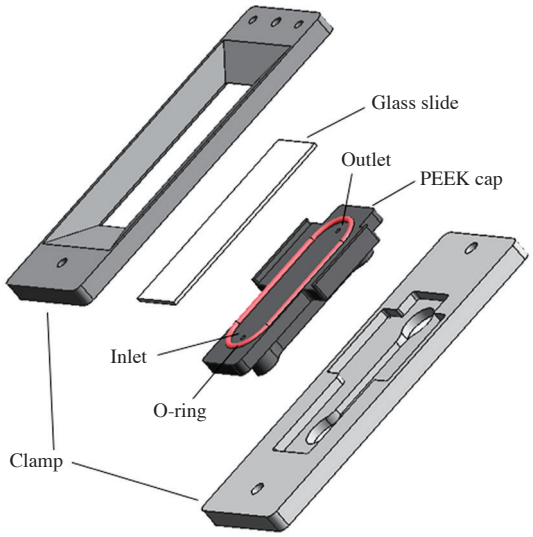

Figure 2. The 3D schematic diagram of flow cell which consists of a clamp, a glass slide, a PEEK cap with 0.5 mm deep fluidic chamber and an o-ring. The fluidic chamber has an inlet at the bottom and an outlet on the top.

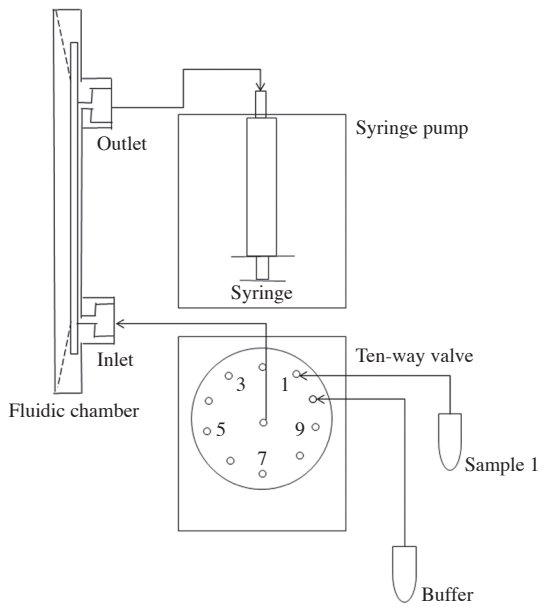

Figure 3. Schematic diagram of fluidic system. The inlet of the fluidic chamber connects to the central port of ten-way selection valve. The outlet connects to the syringe pump.

surfaces of the chamber. Though the friction tends to create an uneven flow across the wide width of a flat chamber when the liquid is evenly pushed upward, the downward gravity compensates for such a propensity. As a result of such a compensation, the liquid moves upward uniformly across the wide width of the chamber and thus across the entire whole microarray.

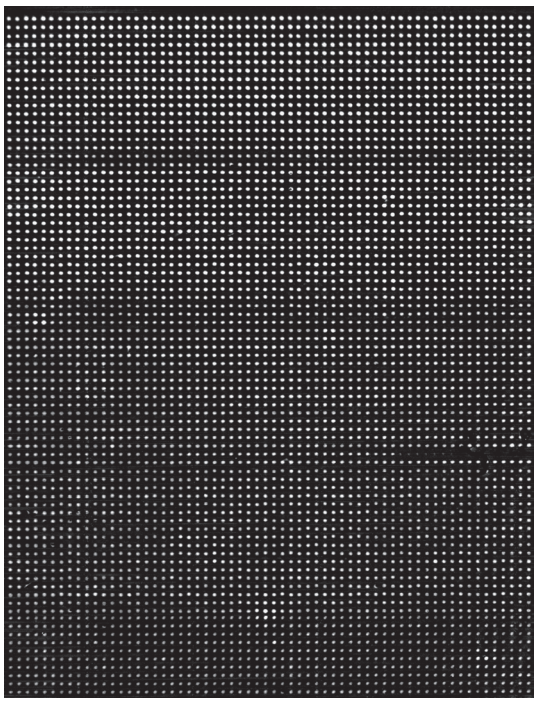

Figure 4. OI-RD image of a microarray consists of 5,022 BBSA. The spot diameter is 100-150 μm and the spot spacing is 250 μm. The microarray covers an area of 1.6 cm × 2.0 cm. The image was acquired after the microarray is washed with 1 × PBS.

In previous fluidic system there are two syringe pumps. One pump is used to withdraw probe solution from liquid reservoirs and push into fluidic chamber and the other pump is used to withdraw 1 × PBS buffer from buffer reservoir and push into fluidic chamber. There is also one 10-way selection valve for up to 10 different probes selection and one injection valve for buffer or probe connection with fluidic chamber selection[22,23]. Compared to previous design of fluidic chamber and fluidic system, the current fluidic chamber and fluidic system has the advantage of: (1) moving the liquid uniformly across the entire microarray by removing the problem of insufficient liquid flow around the corner; (2) avoiding air bubble formation around corners; (3) selection of up to 10 probe solutions with simplified fluidic system consists of one syringe pump and one liquid selection valve.

Results and Analysis

Figure 4 shows the OI-RD image of the microarray in 1 × PBS after excess printed material was washed

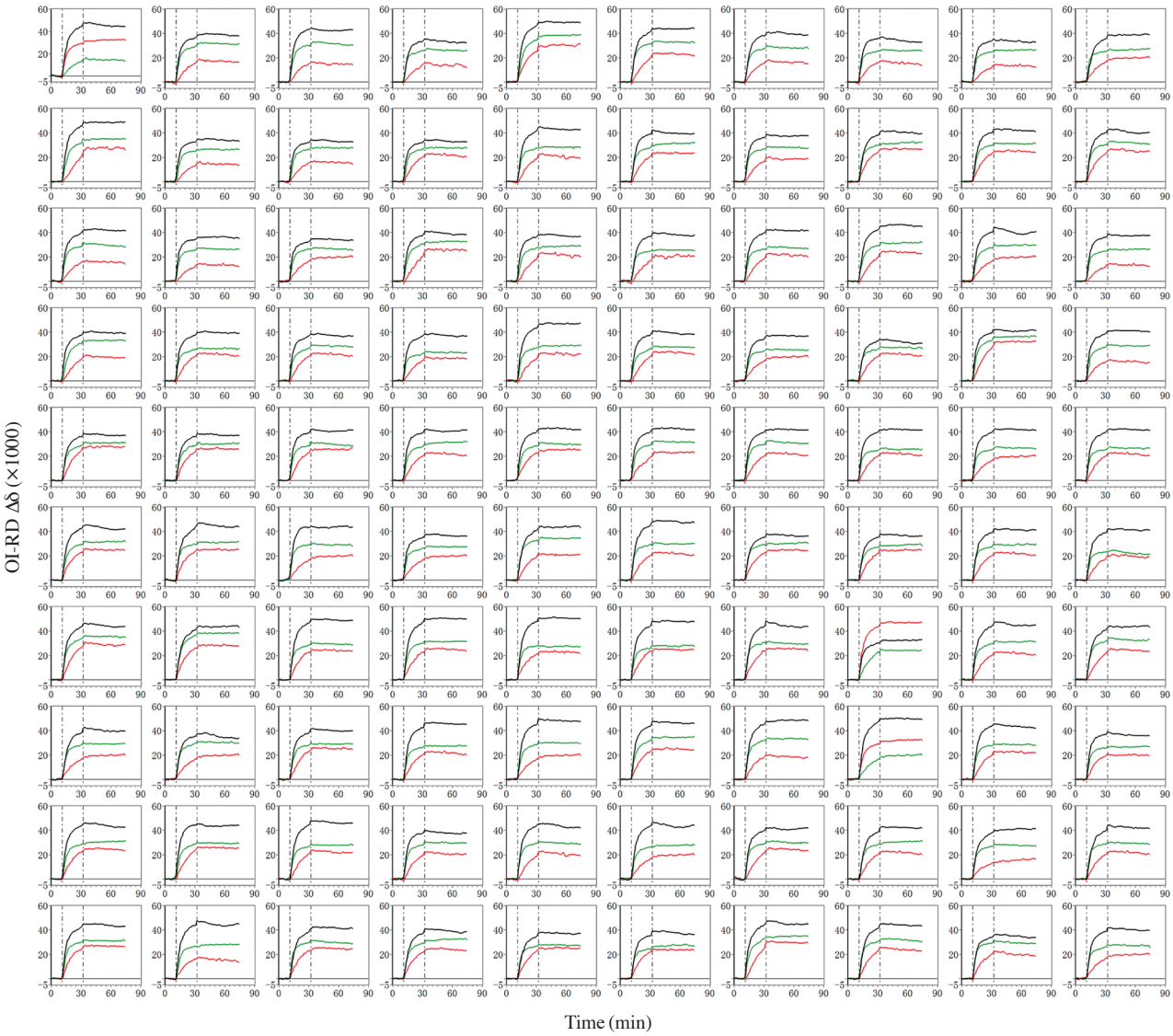

Figure 5. 100 out of 5,022 binding curve sets of anti-biotin IgG binding to BBSA microarray. After a 10 min baseline measurement, the association reaction was measured for 20 min and the dissociation reaction was measured for 40 min. Three curves (red curve = 31.2 nM, green curve = 62.5 nM, black curve = 125 nM) are acquired separately from three fresh microarrays.

off. The image area is 1.6 cm × 2.0 cm. To get accurate equilibrium dissociation constants, on three fresh biotin bovine serum albumin (BBSA) microarrays we performed three binding assays at respective anti-biotin IgG concentrations of 31.2 nM, 62.5 nM and 125 nM in 1 × PBS on three days. We then combined three binding curves of spots with the same microarray coordinates out of three microarrays together as one binding set. Figure 5 shows 100 binding sets, out of 5,022 simultaneously acquired sets. Association and dissociation rate constants were obtained by globally analyzing the binding curve sets using one-to-one Langmuir reaction model. In this model one solution-phase probe is assumed to bind to one surface-immobilized target at a rate proportional to the probe concentration C, $k_{on}C$. Then the captured probes can dissociate from probe-target complexes at a rate of k_{off}, independent of C. When the probe solution is introduced to the microarray at $t = 0$ and then replaced with 1 × PBS at a later time $t = t_0$, the number of captured probes per unit target area is

$$N(t) = N_0 \frac{k_{on}C}{k_{on}C + k_{off}} \left(1 - e^{-(k_{on}C + k_{off})t}\right) \quad t < t_0 \qquad (2)$$

$$N(t) = N_0 \frac{k_{on}C}{k_{on}C + k_{off}} \left(1 - e^{-(k_{on}C + k_{off})t_0}\right) e^{-k_{off}(t-t_0)} \quad t > t_0 \ (3)$$

N_0 is the maximum number of probes that can be captured per unit target area. It depends on many factors such as target density, geometric shapes and orientations of targets and probes so that N_0 is different for each curve. The OI-RD signal $\Delta\delta$ is proportional to N(t) so that we extracted rate constants k_{on} and k_{off} by fitting binding curve sets to Equations (2) and (3) with these two constants as global parameters and N_0 as a local parameter that varies from curve to curve. We computed the equilibrium dissociation constants $K_D = k_{off} / k_{on}$ from the fitting parameters k_{on} and k_{off} for all 5,022 reactions.

In Figure 6, the equilibrium dissociation constant K_D of mouse anti-biotin IgG reaction with 5,022 targets is displayed in the same layout as the target microarray. The equilibrium dissociation constants of 5,022 binding reactions have a mean of 1.6 nM, which is close to values done by other research groups[22,37,38]. The uniform equilibrium dissociation constants distribution across the whole microarray indicates that insufficient liquid flow around the corners has been solved with present fluidic chamber design. In addition, the standard deviation of 5,022 equilibrium dissociation constants is 0.7 nM, indicating that the dot-to-dot deviation, assay-to-assay deviation and day-to-day deviation are small which validates OI-RD system for accurate high-throughput equilibrium dissociation constant measurement.

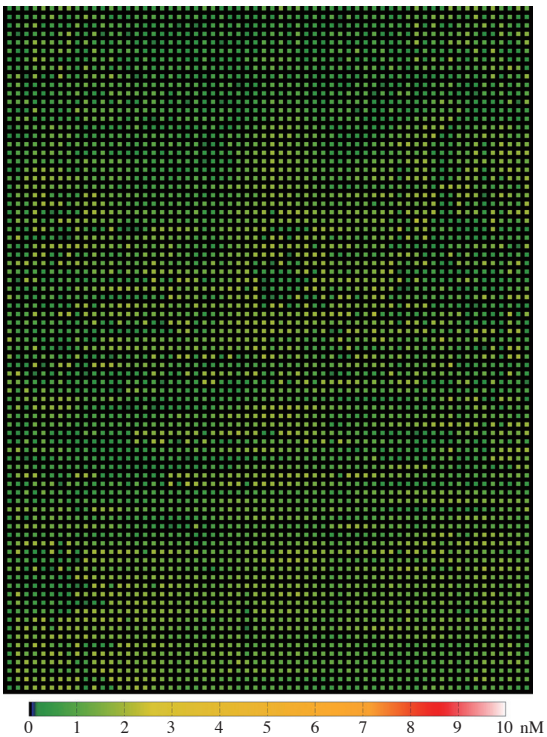

Figure 6. Experimental equilibrium dissociation constants K_D of mouse anti-biotin IgG probe binding to 5,022 BBSA targets, displayed in the same layout as the target microarray (Figure 4).

Discussion and Conclusion

Biomolecular interaction plays important roles in biological systems and the study of reaction rate constants is able to provide information on binding specificity, binding mechanisms, structure-activity relationships, and in turn pathway mapping. Microarrays compatible OI-RD scanning microscopes enables highly parallel studies of reaction rate constants and catches those reactions with high dissociation rates that are easily missed in endpoint assays. To improve fluid transport for accurate reaction rate constant measurement, we demonstrated a flow cell that houses a large microarray with the liquid flowing from the bottom to the top and enables a uniform fluid flow and in turn uniform equilibrium dissociation constants over the entire microarray. The use of one syringe pump, one ten-way liquid selection valve offers a simple fluidic connection for easy and cost effective control.

In addition, the vertical fluid chamber configuration also enables us to increase image and real-time acquisition speed. Two dimensional scanning is adapted to acquire an image or binding curves for the microarray. The laser beam scans vertically with a fast galvanometer along y-axis which takes 0.1 ms for each movement. The fluidic assembly moves horizontally along x-axis with a slow encoded mechanical stage which takes 200 ms for each movement. By making the long side of a rectangular microarray along y-axis, the scan time for image and binding curves is reduced with less time spent on mechanical stage movement.

Materials and Methods

A microarray of $62 \times 81 = 5{,}022$ biotin bovine serum albumin (BBSA, Sigma-Aldrich) was printed at a concentration of 7.6 μM in 1 × phosphate buffered saline (PBS, Sigma-Aldrich) on epoxy-functionalized glass slides (CapitalBio Corporation). The spot diameter is 100-150 μm and the spot spacing is 250 μm. The microarray covers an area of 1.6 cm × 2.0 cm. The printed microarray was washed in situ with 1 × PBS buffer to remove unbound target materials and was incubated in

a solution of 7.6 μM bovine serum albumin (BSA, 0.5 mg/mL) for 30 min to cover the unprinted surface. For parallel detection of 5,022 binding reactions, we used mouse anti-biotin IgG (Jackson ImmunoResearch) as the probe of interest and measured a baseline with microarray in 1 × PBS buffer for 10 min. We then replaced the buffer with an anti-biotin solution at 5 mL/min in 18 sec. The flow rate of the solution was then reduced to 0.05 mL/min for 20 min (association phase of the reaction). Finally we replaced the anti-biotin solution with 1 × PBS buffer at 5 mL/min in 18 sec and then reduced the flow rate of the buffer to 0.05 mL/min for 40 min (dissociation phase of the reaction). We acquired OI-RD images of the microarray before and after the reaction for endpoint analysis.

For microarray detection, we use an f-theta lens to focus the incident laser beam into a spot of a diameter of 20 μm on the back surface of the glass slide. Imaging of microarray is achieved by two-dimensional scanning which is composed of raster scanning of the focus beam across the microarray with a galvanometer along the y-axis (vertical direction) and moving of microarray fluidic assembly along the x-axis (horizontal direction) with a translation stage. The step sizes along two directions are both 20 μm. The scan range of an f-theta lens along y-axis is 2.0 cm.

To simultaneously measure binding curves of a probe to the immobilized targets, we perform repeated scans of a subset of pixels on the microarray surface. We select one pixel from each target spot as the signal channel and two pixels on the unprinted region as the reference channels, which lie in between two target spots along vertical direction. Each reference channel is shared by two neighboring signal channels. The optical signal Δδ from a signal channel minus the averaged optical signal from the two neighboring reference channels yields the background-corrected signal for the target.

Acknowledgements This work is supported by the NSFC (Grant No.61505032, 11574056, 61575046, 31500599), the Open Foundation of the State Key Laboratory of Modern Optical Instrumentation, Science and Technology Commission of Shanghai Municipality (Shanghai Rising-Star Program, Grant No. 16QA1400400).

References

1. Schena, M., Shalon, D., Davis, R.W. & Brown, P.O. Quantitative monitoring of gene-expression patterns with a complementary-DNA micro. *Science* **270**, 467-470 (1995).
2. Stoughton, R.B. Applications of DNA microarrays in biology. *Annu. Rev. Biochem.* **74**, 53-82 (2005).
3. MacBeath, G. Protein microarrays and proteomics. *Nat. Genet.* **32**, 526-532 (2002).
4. Stoevesandt, O., Taussig, M.J. & He, M.Y. Protein microarrays: high-throughput tools for proteomics. *Expert Rev. Proteomics* **6**, 145-157 (2009).
5. Feizi, T., Fazio, F., Chai, W.C. & Wong, C.H. Carbohydrate microarrays - a new set of technologies at the frontiers of glycomics. *Curr. Opin. Struct. Biol.* **13**, 637-645 (2003).
6. Song, X.Z. *et al*. Shotgun glycomics: a microarray strategy for functional glycomics. *Nat. Methods* **8**, 85-U125 (2011).
7. Andersen, M.R. *et al*. A trispecies aspergillus microarray: comparative transcriptomics of three aspergillus species. *Proc. Natl. Acad. Sci. U. S. A.* **105**, 4387-4392 (2008).
8. Gobert, G.N. *et al*. Transcriptomics tool for the human Schistosoma blood flukes using microarray gene expression profiling. *Exp. Parasitol.* **114**, 160-172 (2006).
9. Phelps, T.J., Palumbo, A.V. & Beliaev, A.S. Metabolomics and microarrays for improved understanding of phenotypic characteristics controlled by both genomics and environmental constraints. *Curr. Opin. Biotechnol.* **13**, 20-24 (2002).
10. Soanes, K.H. *et al*. Molecular characterization of zebrafish embryogenesis via DNA microarrays and multiplatform time course metabolomics studies. *J. Proteome Res.* **10**, 5102-5117 (2011).
11. Zhu, H. *et al*. Global analysis of protein activities using proteome chips. *Science* **293**, 2101-2105 (2001).
12. Sun, Y.S., Landry, J.P., Fei, Y.Y. & Zhu, X.D. Effect of fluorescently labeling protein probes on kinetics of protein-ligand reactions. *Langmuir* **24**, 13399-13405 (2008).
13. Rich, R.L. & Myszka, D.G. Survey of the year 2007 commercial optical biosensor literature. *J. Mol. Recognit.* **21**, 355-400 (2008).
14. Singh, B.K. & Hillier, A.C. Surface plasmon resonance imaging of biomolecular interactions on a grating-based sensor array. *Anal. Chem.* **78**, 2009-2018 (2006).
15. Hanel, C. & Gauglitz, G. Comparison of reflectometric interference spectroscopy with other instruments for label-free optical detection. *Anal. Bioanal. Chem.* **372**, 91-100 (2002).
16. Ozkumur, E. *et al*. Label-free and dynamic detection of biomolecular interactions for high-throughput microarray applications. *Proc. Natl. Acad. Sci. U. S. A.* **105**, 7988-7992 (2008).
17. Cross, G.H. *et al*. The metrics of surface adsorbed small molecules on the Young's fringe dual-slab waveguide interferometer. *J. Phys. D: Appl. Phys.* **37**, 74-80 (2004).
18. Wang, Z.H. & Jin, G. A label-free multisensing immunosensor based on imaging ellipsometry. *Anal. Chem.* **75**, 6119-6123 (2003).
19. Arwin, H. Ellipsometry on thin organic layers of biological interest: characterization and applications. *Thin*

Solid Films **377**, 48-56 (2000).
20. Nand, A. *et al*. In situ protein microarrays capable of real-time kinetics analysis based on surface plasmon resonance imaging. *Anal. Biochem*. **464**, 30-35 (2014).
21. Boozer, C., Kim, G., Cong, S.X., Guan, H.W. & Londergan, T. Looking towards label-free biomolecular interaction analysis in a high-throughput format: a review of new surface plasmon resonance technologies. *Curr. Opin. Biotechnol*. **17**, 400-405 (2006).
22. Landry, J.P., Fei, Y.Y. & Zhu, X.D. Simultaneous Measurement of 10,000 Protein-Ligand Affinity Constants Using Microarray-Based Kinetic Constant Assays. *Assay Drug Dev. Technol*. **10**, 250-259 (2012).
23. Landry, J.P., Proudian, A.P., Malovichko, G. & Zhu, X.D. Kinetic identification of protein ligands in a 51,200 small-molecule library using microarrays and a label-free ellipsometric scanner. In Proceedings of SPIE BIOS 2013, Imaging, Manipulation, and Analysis of Biomolecules, Cells, and Tissues XI, 8587 IV. SPIE-Int Soc. Opt. Eng. (2013).
24. Zhu, C.G. *et al*. Calibration of oblique-incidence reflectivity difference for label-free detection of a molecular layer. *Appl. Opt*. **55**, 9459-9466 (2016).
25. Nabighian, E., Bartelt, M.C. & Zhu, X.D. Kinetic roughening during rare-gas homoepitaxy. *Phys. Rev. B*. **62**, 1619-1622 (2000).
26. Thomas, P., Nabighian, E., Bartelt, M.C., Fong, C.Y. & Zhu, X.D. An oblique-incidence optical reflectivity difference and LEED study of rare-gas growth on a lattice-mismatched metal substrate. *Appl. Phys. A*. **79**, 131-137 (2003).
27. Zhu, X.D., Wicklein, S., Gunkel, F., Xiao, R. & Dittmann, R. In situ optical characterization of $LaAlO_3$ epitaxy on $SrTiO_3$(001). *Europhys. Lett*. **109**, 37006 (2015).
28. Schwarzacher, W., Gray, J.W. & Zhu, X.D. Oblique incidence reflectivity difference as an in situ probe of Co electrodeposition on polycrystalline Au. *Electrochem. Solid-State Lett*. **6**, C73-C76 (2003).
29. Wu, G.Y. *et al*. Pb electrodeposition on polycrystalline Cu in the presence and absence of Cl^-: A combined oblique incidence reflectivity difference and in situ AFM study. *Surf. Sci*. **601**, 1886-1891 (2007).
30. Fei, Y.Y. *et al*. Characterization of receptor binding profiles of influenza A viruses using an ellipsometry-based label-free glycan microarray assay platform. *Biomolecules* **5**, 1480-1489 (2015).
31. Fei, Y.Y. *et al*. Use of real-time, label-free analysis in revealing low-affinity binding to blood group antigens by Helicobacter pylori. *Anal. Chem*. **83**, 6336-6341 (2011).
32. Landry, J.P. *et al*. Discovering Small Molecule Ligands of Vascular Endothelial Growth Factor That Block VEGF-KDR Binding Using Label-Free Microarray-Based Assays. *Assay Drug Dev. Technol*. **11**, 326-332 (2013).
33. Fei, Y.Y. *et al*. A novel high-throughput scanning microscope for label-free detection of protein and small-molecule chemical microarrays. *Rev. Sci. Instrum*. **79**, 013708 (2008).
34. Guo, X.X. *et al*. Characterization of protein expression levels with label-free detected reverse phase protein arrays. *Anal. Biochem*. **509**, 67-72 (2016).
35. Wang, J.J. *et al*. Epigallocatechin-3-gallate (EGCG) enhances ER stress-induced cancer cell apoptosis by directly targeting PARP16 activity. *Cell Death Discov*. **3**, e17034 (2017).
36. Zhu, C.G. *et al*. Developing an Efficient and General Strategy for Immobilization of Small Molecules onto Microarrays Using Isocyanate Chemistry. *Sensors* **16**, 378 (2016).
37. Jung, H.S. *et al*. Impact of hapten presentation on antibody binding at lipid membrane interfaces. *Biophys. J*. **94**, 3094-3103 (2008).
38. Zhang, N. *et al*. Plasmonic metal nanostructure array by glancing angle deposition for biosensing application. *Sens. Actuators B-Chem*. **183**, 310-318 (2013).